Journal of Alloys and Compounds, 191 (1993) 15–19
JALCOM 395

X-ray diffraction analysis of Ti-diffused single-crystal $LiNbO_3$

Perry Skeath*
Optical Sciences Division, Naval Research Laboratory, Washington, DC 20375-5000 (USA)

S. B. Qadri
Condensed Matter and Radiation Sciences Division, Naval Research Laboratory, Washington, DC 20375-5000 (USA)

F. A. Stevie
AT&T Bell Laboratories, Allentown, PA 18103 (USA)

(Received June 29, 1992)

Abstract

Lattice changes due to Ti diffusion into single crystal $LiNbO_3$ have been characterized by double crystal rocking curve measurements using the $(220)_{hex}$, $(226)_{hex}$, and $(00\underline{12})_{hex}$ reflections. Narrow full width at half-maxima of these reflections observed at low Ti concentrations indicate a high degree of lattice uniformity despite a substantial intrinsic defect density. The ***a*** lattice parameter of $LiNbO_3$ varies bilinearly with Ti concentration, while the ***c*** lattice parameter variation is nearly zero. This result is consistent with a concentration-dependent Ti site in $LiNbO_3$. The break in the bilinear function of the ***a*** lattice parameter occurs between a Ti concentration of 3% and 6% of the Li or Nb lattice sites. This strongly suggests that the Ti, below a concentration of 6%, replaces the Nb which is located in approximately 6% of the Li sites of congruent $LiNbO_3$. The maximum solubility of Ti in $LiNbO_3$ (at 1050 °C) is deduced from the maximum change in ***a*** lattice parameter.

1. Introduction

The Ti:$LiNbO_3$ system is commonly used in the fabrication of optical waveguide switches, modulators, and other devices. Several excellent references which review the physics and chemistry of congruent $LiNbO_3$ are available [1]. The diffusion of Ti into single crystal $LiNbO_3$ from a metallic film has been found to proceed in three basic steps: (i) oxidation of the Ti; (ii) reaction of the Ti with the $LiNbO_3$ to form a "source compound"; and (iii) diffusion from the "source compound" reacted layer into $LiNbO_3$ lattice, accompanied by a small amount of $LiNbO_3$ epitaxial regrowth [2]. A consensus on the "source compound" composition has not yet emerged [3].

Sugii *et al.* [4] performed X-ray rocking curve measurements on Ti-diffused single crystal *y*-cut $LiNbO_3$ and reported a lattice contraction along the ***a***-axis: $\Delta a/a \approx 10^{-3}$. As a result of the cut of their crystals, they were unable to measure $\Delta c/c$ directly. Guenais *et al.* [5] have studied the phase equilibria and lattice parameters of TiO_2:$LiNbO_3$ sintered powders. They determined a solubility limit of approximately 20% at a temperature of 1187 °C (18% at 1050 °C by interpolation of their data), and found that the lattice contraction $\Delta a/a \approx 1.9 \times 10^{-3}$ ($x = 0.1$, x being the mole fraction of TiO_2). Guenais *et al.* were unable to determine $\Delta c/c$ accurately within the error of their measurement ($\pm 0.01°$) owing to the small magnitude of $\Delta c/c \leqslant 0.5 \times 10^{-3}$ ($x = 0.1$). Franzosi *et al.* [6], using X-ray rocking curve, X-ray topography, and transmission electron microscopy methods, also observed a marked contraction of the ***a*** lattice parameter and related that to misfit dislocations.

It is of particular interest to go beyond merely measuring a change in lattice parameters, and relate the Ti lattice site to the change in optical indices. Sugii *et al.* [4] attempted to do this, but their conclusion that the change in lattice parameter was the source of the change in optical index did not seem consistent with other data. In an earlier experiment, we used extended X-ray absorption fine structure (EXAFS) and X-ray absorption near edge structure (XANES) methods [7] on Ti-diffused $LiNbO_3$ to characterize the local site of the Ti in the $LiNbO_3$ lattice [8]. The local environment of the Ti site was found to be concentration dependent, and the resulting change in the local Ti bond orbitals was related directly to the bilinear behavior of the optical index. In the present investigation, we extend

*On assignment from SFA, Inc. (currently at ITM, Inc., 1113 Dennis Avenue, Silver Spring, MD 20901, USA).

0925-8388/93/$6.00

the previous work to a systematic study of the $LiNbO_3$ lattice parameters (in the ferroelectric phase with C_{6v} symmetry [1]) as a function of Ti concentration.

2. Experimental details

The source material consisted of *x*-cut and *z*-cut congruent single crystal optical quality $LiNbO_3$ obtained from Crystal Technology, Inc. (Palo Alto, CA, USA). Ti was sputter deposited in Ar from an RF magnetron source. An accurate determination of the amount of Ti deposited was critical for this experiment. The approach taken was to measure the film's average thickness in terms of the Ti atoms deposited per square centimeter (at cm^{-2}) by a calibrated optical transmission method [9]. Calibration was performed using Rutherford backscattering spectroscopy (RBS) with an absolute accuracy of 1%. Conversion of the thickness from Ti atoms deposited per square centimeter (at cm^{-2}) to Ångstroms (Å) was done by assuming a film density equal to the bulk density of 4.50 g/cm^{-3}; the conversion factor is 5.66×10^{14} Ti at cm^{-2} Å. The film thicknesses ranged in steps from 38 Å to 1627 Å. Ti diffusion was carried out in a quartz tube Lindberg furnace at 1050 °C. Since H_2O is thought to suppress the loss of Li during diffusion, *x*-cut samples of the same Ti thickness were diffused for 2.5 h in either wet or dry oxygen ambients to assess the role of H_2O in the Ti diffusion and incorporation into the lattice. *Z*-cut samples were diffused only in dry oxygen, for 3.5 h. These diffusions are only half as deep as the typical optical waveguide diffusion so that a substrate peak would be clearly visible in the diffraction data.

The optical transmission method yielded a precise measure of the amount of Ti deposited, and therefore also gave a relative measure of the Ti surface concentration after diffusion. Secondary ion mass spectrometry (SIMS) was performed on samples with the most Ti deposited to calibrate the Ti near-surface atomic concentration and to determine if any reacted compound remained after the diffusion. SIMS depth profiles were obtained with a Perkin–Elmer (Physical Electronics Division) model PHI-300 with a 6 keV. 0.6 mA O_2^+ primary beam rastered over a 500×500 mm area and change neutralized with a 12 mA electron beam. An average sputter rate of 150 Å min^{-1} was achieved. Quantitation was made possible with a double-isotope implant of ^{48}Ti and ^{50}Ti in $LiNbO_3$. Normalization to the Nb matrix signal was used to determine the Ti signal both in the diffused region of the $LiNbO_3$ crystal and in any remaining diffusion source layer at the surface. Thus the accuracy of diffused Ti atomic concentration in absolute terms is limited by the accuracy of the SIMS quantitation, which is on the order of ±50% of the measured concentration.

Some confusion may arise as a result of the different conventions used for indexing X-ray diffraction beams and tensor properties of $LiNbO_3$. Crystallographers use hexagonal coordinates $(a_1\ a_2\ c)_{hex}$ to index axes and X-ray diffraction peaks. However, a cartesian coordinate system $(x\ y\ z)_{cart}$ is used for tensor properties such as the linear electro-optic effect, and hence is the coordinate system used by researchers who fabricate optical waveguides (and by their crystal suppliers). The following convention is commonly used to assign cartesian coordinates: the *z* axis is parallel to the *c* axis, the *x* axis is parallel to one of the equivalent *a* axes (a_1, a_2, or a_3), and the *y* axis is chosen such that the system is right-handed [1]. Those who are interested in device-related properties use the cartesian coordinate system exclusively, hence the reference to *x*-cut and *y*-cut crystals. Since both diffraction data and tensor properties are discussed below, we make reasonable efforts to identify which coordinate system is referred to in this paper – hexagonal coordinates, when referred to in the text below, are followed with a subscript hex, such as $(220)_{hex}$. The ***a*** lattice parameter of congruent $LiNbO_3$ is given in the literature as 5.1483 Å, and the corresponding ***c*** lattice parameter is 13.867 Å.

Cu $K\alpha_1$ radiation was used for all diffraction measurements. The X-ray rocking curve measurements were performed using a double crystal spectrometer in the parallel (+,−) configuration. A nearly perfect $LiNbO_3$ crystal was used as the first crystal. Two reflections, $(220)_{hex}$ and $(226)_{hex}$, were used for analysis of *x*-cut crystals, and $(00\underline{12})_{hex}$ and $(226)_{hex}$ for *z*-cut crystals. For the symmetric reflections $(220)_{hex}$ and $(00\underline{12})_{hex}$ only one measurement was made. Two measurements were made for the asymmetric reflection $(226)_{hex}$. In one asymmetric measurement the angle of incidence was $\theta-\phi$ while in the second measurement the angle of incidence was $\theta+\phi$, where ϕ is the inclination of the near-surface Ti-diffused lattice planes with respect to the undiffused bulk crystal lattice planes. From these measurements, $\Delta\theta$ (the difference in the Bragg angles of the substrate and the near-surface Ti-diffused region, due to differences in layer spacing) and $\Delta\phi$ were obtained precisely. The minimum full width at half-maximum (FWHM) of reflections from undiffused samples (samples without Ti) were 7 s for the $(220)_{hex}$ reflection and 5 s for the $(226)_{hex}$ reflection. Therefore the resolution of the double crystal spectrometer in the parallel (+,−) configuration was estimated to be on the order of 5 s of arc or less, corresponding to a lattice parameter resolution of 0.00012 Å using the $(220)_{hex}$ reflection and ***a***,***c*** lattice parameter resolution of 0.00037 Å using the $(0012)_{hex}$ reflection. However,

the peak separation resolution was found to be about 2 s of arc based on the reproducibility of substrate and diffused-layer peak separation measurements.

SIMS depth profiles of selected samples diffused in either wet or dry oxygen revealed a smooth gaussian diffusion profile with no evidence of a Ti-rich surface layer. The diffusion is regarded as complete as a result of the absence of a Ti-rich surface layer [8]. The selected samples were processed as follows: 3.48×10^{17} Ti at cm^{-2} (614 Å) was deposited on sample LNX-03 (*x*-cut $LiNbO_3$) which was then diffused for 2.5 h at 1050 °C in dry oxygen. This resulted in a Ti near-surface atomic concentration of 2.5×10^{21} Ti at cm^{-3} ($\pm1.3\times10^{21}$ Ti at cm^{-3}) in LNX-03, as measured by SIMS. 3.66×10^{17} Ti at cm^{-2} (646 Å) was deposited on sample LNX-19 (*x*-cut $LiNbO_3$) which was then diffused for 2.5 h at 1050 °C in wet oxygen. This resulted in a Ti surface concentration of 3.0×10^{21} Ti at cm^{-3} ($\pm\approx1.5\times10^{21}$ Ti at cm^{-3} in LNX-19, as measured by SIMS. Sample LNZ-44 (*z*-cut $LiNbO_3$) was diffused for 3.5 h at 1050 °C in dry oxygen, resulting in a Ti surface concentration of 1.6×10^{21} Ti at cm^{-3} ($\pm\approx0.8\times10^{21}$ Ti at cm^{-3}), as measured by SIMS.

3. Results and discussion

Diffraction data were first obtained using the $(220)_{hex}$ reflection (*x*-planes spaced *a*/2 apart) from *x*-cut $LiNbO_3$. Bragg reflections from undoped $LiNbO_3$ crystals were quite narrow: 20 cm or less FWHM for the $(220)_{hex}$ peak. Dry-oxygen Ti-diffused samples showed a second diffraction peak at increased diffraction angles (see Fig. 1). At the lowest Ti surface concentrations this shifted peak was accompanied by a weak auxiliary structure between the shifted peak and the substrate peak; this may be Pendellosung fringes. This second peak shifted toward larger diffraction angles and broadened as the surface concentration of Ti increased. The substrate peak also broadened as the surface concentration of Ti increased. Wet oxygen Ti-diffused samples showed very similar behavior (except for the sample having the largest Ti concentration). Similarly, a second peak appeared in the $(226)_{hex}$ rocking curve which broadened and shifted away from the substrate peak as the Ti concentration was increased (these data will be shown in a more lengthy paper), with no large difference between samples diffused in wet *vs.* dry oxygen.

The change in the $LiNbO_3$ *a* lattice parameter was extracted from the $(220)_{hex}$ rocking curve data as a function of surface Ti concentration for the samples diffused in wet oxygen and those diffused in dry oxygen. The data show a decrease of the *a* lattice parameter as the surface Ti concentration is increased (see Fig. 2). The *a* lattice parameter was never observed to fall below a value of 5.1350 Å despite further increases in Ti concentration, indicating an apparent saturation of the solid solubility at a Ti concentration of approximately 4×10^{21} Ti at cm^{-3} (a Ti density equal to approximately 21% of the niobium lattice sites, 1.89×10^{22} Nb at cm^{-3}). It should be noted that the surfaces of all samples were free of "haze" after diffusion except for the samples having the highest Ti concentration (corresponding to Ti concentrations exceeding the solid solubility limit).

Examination of the *a* lattice parameter variation for dry-oxygen-diffused samples reveals two distinct regions or domains below the solubility limit: a low-concen-

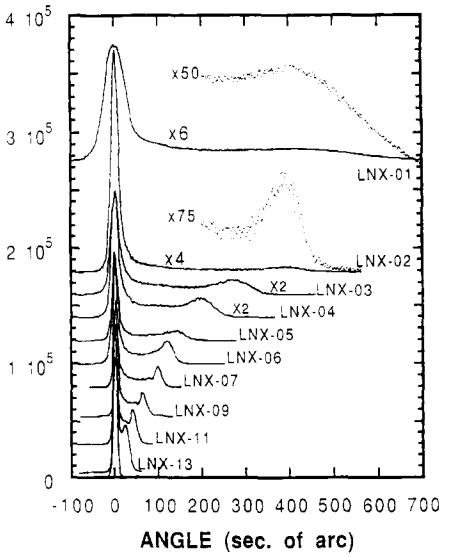

Fig. 1. $(220)_{hex}$ rocking curves (*x*-cut Ti:$LiNbO_3$; dry).

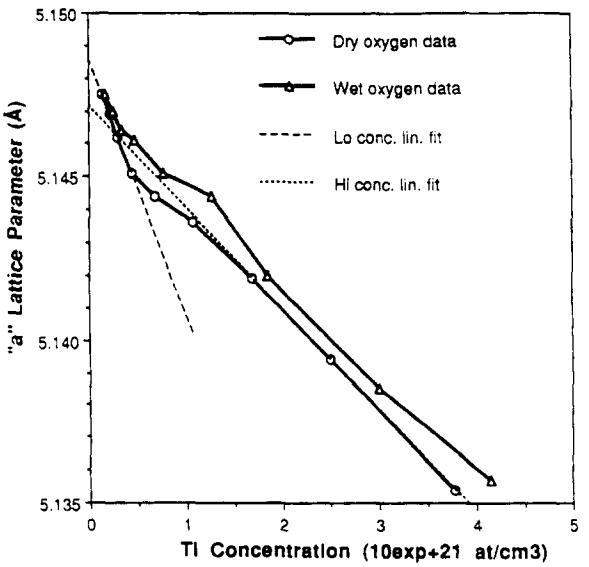

Fig. 2. Variation of the *a* lattice parameter as a function of Ti atomic concentration. The linear relationships for the low and high concentration regions are shown with dashed lines.

tration region and a high-concentration region. The low-concentration region is characterized by a simple linear dependence between the *a* lattice parameter and the Ti concentration: *a* (in ångstroms) = $5.1486 - 0.00148x$ (percentage of Ti). This linear relationship for the low-concentration region of dry-oxygen-diffused samples is valid up to 2.4% Ti (approximately 4×10^{20} Ti at cm^{-3}). Between 2.4% Ti and 5.6% Ti (approximately 1×10^{21} Ti at cm^{-3}) there is a transition to the high-concentration regime. The high concentration region of dry-oxygen-diffused samples, between 5.6% and the solid solubility limit, is characterized by a second linear relationship: *a* (in ångstroms) = $5.14715 - 0.000584x$ (percentage of Ti).

The presence of H_2O vapor during $LiNbO_3$ diffusion influences the variation in the *a* lattice parameter. The most obvious effects of the H_2O seem to be to suppress slightly the *a* lattice parameter variation, particularly around the transition between the low- and high-concentration regions, and to blur the distinction between the low- and high-concentration regions (see Fig. 2). The data points for the wet-oxygen-diffused samples also appear to be somewhat more scattered, in contrast to the very smooth curve defined by data points for the dry-oxygen-diffused samples.

Diffraction data were then obtained using the $(00.\underline{12})_{hex}$ reflection (*z*-planes spaced *c*/12 apart) from *z*-cut $LiNbO_3$. Dry-oxygen Ti-diffused samples showed only a single diffraction peak corresponding to the substrate peak position at all Ti concentrations (see Fig. 3). Rocking curves from two samples did show one or even two additional peaks, but these peaks were sensitive to alignment, their positions did not vary systematically from one sample to the other, and the peaks were not reproducible. As the Ti concentration was increased the single diffraction peak broadened, as in the case of the $(220)_{hex}$ and $(226)_{hex}$ substrate and diffused layer diffraction peaks. Thus there is the unusual result that even at very high Ti concentrations the change in the *c* lattice parameter is so small as to

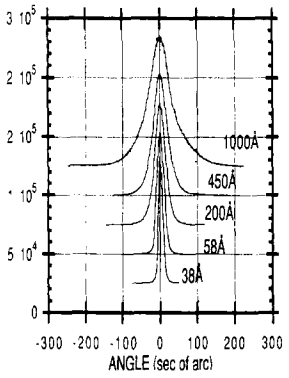

Fig. 3. $(00\underline{12})_{hex}$ rocking curves (*z*-cut Ti:$LiNbO_3$; dry).

be undetectable by a double crystal spectrometer using nearly perfect $LiNbO_3$ crystals.

The first result obtained was that the diffraction peaks from undiffused congruent $LiNbO_3$ crystals were quite narrow, with FWHM averaging about 7–8 s of arc for the $(220)_{hex}$ reflection. The narrow diffraction peak widths imply (i) a very low degree of internal strain; and (ii) a high degree of uniformity. This was surprising in view of the intrinsic non-stoichiometry, the mechanical polishing used to finish the surface, and the strong polarization of the crystals.

The $(220)_{hex}$ diffraction data show very clearly the limit imposed by the solid solubility of TiO_2 in $LiNbO_3$. There is quite good agreement between the solid solubility limit of $x \approx 0.18$ (x being the mole fraction of TiO_2) at 1050 °C anticipated by Guenais using TiO_2:$LiNbO_3$ sintered powders (interpolated from Fig. 3(a) in Guenais *et al.* [5]) and the solid solubility limit of $x \approx 0.21$ at 1050 °C found in the data above using single-crystal Ti diffused congruent $LiNbO_3$.

The $(220)_{hex}$ diffraction data from dry-oxygen-diffused samples also show a bilinear dependence of the *a* lattice parameter on the Ti concentration below the solid solubility limit. This was not totally unexpected owing to our earlier results from EXAFS data [8] showing that the Ti center in dry-oxygen-diffused congruent $LiNbO_3$ undergoes a change in the *x*-planes between a Ti concentration approximately of 5×10^{20} Ti at cm^{-3} and 2×10^{21} at cm^{-3}. There is also the bilinear dependence of the ordinary optical index (which is also associated with the *x*-planes) on Ti concentration, which has been reported by several independent workers [10]. Ctyroky, for example, shows an abrupt decrease in the slope of the ordinary index occurring in the Ti mass concentration range 0.2%–0.7% (approximately 1.3×10^{20} Ti at cm^{-3} to approximately 4×10^{20} Ti at cm^{-3}). The transition between low- and high-concentration regions observed in the $(220)_{hex}$ diffraction data occurs within approximately the same range, between a Ti concentration of approximately 4×10^{20} Ti at cm^{-3} and approximately 1×10^{21} Ti at cm^{-3}.

The problem of the Ti site in the $LiNbO_3$ lattice is complex, due in large part to the nonstoichiometry, disorder [11] and inherent defect structure [12] of $LiNbO_3$ with congruent composition. One might expect that since Ti^{4+} and Nb^{5+} are of very similar size, charge, and bond orbital configuration, Ti would naturally substitute for Nb on Nb sites. By this elementary reasoning, Pearsall *et al.* proposed that since they were able to detect only Ti in the 4+ oxidation state at the $LiNbO_3$ source, the Ti was probably on the Nb lattice site [13]. However, it has been known for many years that congruent $LiNbO_3$ accommodates its excess of Nb by placing Nb on Li sites: experimental evidence indicates that approximately 6% of the Li lattice sites

in $LiNbO_3$ are occupied by Nb atoms [14] with charge balance accomplished by associated vacancies or other defects. Thus when three experimentally observed facts are taken together – the excess Nb of congruent $LiNbO_3$ on 6% of the Li sites, the lower charge state of Ti compared with Nb, and the change in the Ti incorporation site occurring between 3% and 6% – they suggest strongly that Ti replaces Nb in Li lattice sites in the low-concentration region. The substitution of Ti in Nb in Li sites is also consistent with the strong pre-edge peak referred to earlier [8]. Both the Li and Nb sites are octahedral in ferroelectric $LiNbO_3$, but the Li octahedral symmetry is broken to a larger degree than the Nb octahedral symmetry. The pre-edge peak seen in the low-concentration Ti *l–s* X-ray absorption edge data is associated with broken octahedral symmetry – the stronger the symmetry breaking, the stronger the pre-edge peak. For example, in the series $SrTiO_3$, $BaTiO_3$, and $PbTiO_3$, the pre-edge peak increases linearly with Ti displacement from the octahedral center of symmetry [15]. Another significant result is that the change in the ***c*** lattice parameter as a function of Ti concentration is so small that it is undetectable in our data. There is consistency with the Ti:$LiNbO_3$ EXAFS data, in which no change in the EXAFS amplitude or in the pre-edge peak was observed when X-rays were polarized along the ***c*** axis [8]. The EXAFS data indicated that no change in the local environment of the Ti impurity atom occurred along the ***c*** axis. However, the variation in the extraordinary optical index (associated with the polar ***c*** axis) as a function of Ti concentration is stronger than the variation of the ordinary optical index (associated with the nonpolar ***a*** axis). The source of the change in the ordinary optical index as a function of Ti concentration was indicated in a previous paper: the Ti displacement in the ***xy*** plane was associated with change in the ***xy*** plane Ti states near the conduction band minimum, which are directly related to the ordinary optical index [8]. Based on the data presented in this paper, the change in the extraordinary optical index as a function of Ti concentration is clearly not associated with a change in the ***c*** lattice parameter, but rather is assumed to be due to changes in polarization.

4. Conclusions

The ***a*** lattice parameter of $LiNbO_3$ varies bilinearly with Ti concentration, while the ***c*** lattice parameter variation is nearly zero. The break in the bilinear function of the ***a*** parameter occurs between a Ti concentration of 3% and 6% of the Li or Nb sites. Below a concentration of 6% Ti atoms replace Nb atoms which are located in nearly 6% of the Li sites of congruent $LiNbO_3$.

References

1 R. S. Weis and T. K. Gaylord, *Appl. Phys. A, 37* (1985) 191–203.
A. Rauber, in E. Kaldis (ed.), *Current Topics Mat. Sci.*, Vol. 1, North-Holland, Amsterdam, 1978, pp. 481–601.
Properties of Lithium Niobate, INSPEC, The Institution of Electrical Engineers, London, 1989, EMIS Datareviews Series No. 5.

2 M. DeSario, M. N. Armenise, C. Canali, A. Carnera, P. Mazzoldi and G. Celotti, *J. Appl. Phys., 57* (1985) 1482–1488 and references cited therein.

3 C. E. Rice and R. J. Holmes, *J. Appl. Phys., 60* (1986) 3836–3839.
R. J. Holmes and D. M. Smyth, *J. Appl. Phys., 55* (1984) 3531–3535.
W. K. Burns, P. H. Klein, E. J. West and L. E. Plew, *J. Appl. Phys., 50* (1979) 3063.

4 K. Sugii, M. Fukuma and H. Iwasaki, *J. Mat. Sci., 13* (1978) 523–533.

5 B. Guenais, M. Baudet, M. Minier and M. LeCun, *Mater. Res. Bull., 16* (1981) 643–653.

6 P. Franzosi, P. Sgarzi and E. Zanoni, *Ultramicroscopy, 12* (1983) 116–17.

7 L. V. Azaroff (ed.), *X-Ray Spectroscopy*, McGraw Hill, New York, 1974.
F. W. Lytle, D. E. Sayers and E. A. Stern, in C. Bonnelle and C. Mande (eds.), *Advances in X-ray Spectroscopy*, Pergamon, New York, 1982.
B. K. Teo, *EXAFS: Basic Principles and Data Analysis*, Springer, New York, 1986.

8 P. Skeath, W. K. Burns and W. T. Elam, in T. F. Batchmann *et al.* (eds), *Optoelectronic Materials, Devices, Packaging and Interconnects*, Proc. SPIE 836, 1988, pp. 32–39.
P. Skeath, W. T. Elam, W. K. Burns, F. A. Stevie and T. H. Briggs, *Phys. Rev. Lett., 59* (1987) 1950–1953.

9 P. Skeath and E. J. West (to be submitted).

10 J. Ctyroky, M. Hofman, J. Janta and J. Schrofel, *IEEE J. Quant. Electr., 20*(4) (1984) 400–409.
J. Vollmer, J. P. Nisius, P. Hertel and E. Kratzig, *Appl. Phys. A, 32* (1983) 125–127.
M. Minakata, S. Saito, M. Shibata and S. Miyazawa, *J. Appl. Phys., 49*(9) (1978) 4677–4682.
K. Ziling, L. Pokrovskiy, V. Shashkin and D. Shipilova, *Avtometriya* (1978) 103–108 (in Russian).

11 D. C. Douglass and G. E. Peterson, *J. Am. Ceram. Soc., 69* (1986) 48–52.

12 D. M. Smyth, *Proc. SPIE, 460* (1984) 22–25.

13 T. P. Pearsall, S. Chiang and R. V. Schmidt, *J. Appl. Phys., 47* (1976) 4794–4797.

14 S. C. Abrahams and P. Marsh, *Acta Crystallogr. Sect B, 42* (1986) 61–68.

15 W. T. Elam, personal communication (data to be published).